ITO-Free Indoor OPV Modules from Nonhalogenated Solvents

*David Müller, Laura Campos Guzmán, Ershuai Jiang, Birger Zimmermann, and Uli Würfel**

The growing market of the internet-of-things (IoT) accelerates the development of indoor organic photovoltaics. Very high performances up to 29% are already achieved under illumination with white light-emitting diodes with intensities in the range of 500–1000 lux. However, topics relevant for mass production such as large area coating, use of nontoxic solvents, and inexpensive electrodes are hardly addressed thus far. Herein this work, an indium-tin-oxide-free device stack is presented, which shows very good performance with many novel absorber materials under both full sun light as well as indoor illumination. Furthermore, lab-scale cells are upscaled to small modules that can power typical IoT devices. This includes the transition from spin coating to slot-die coating as well as the use of green solvents. Further, as the parallel resistance (R_P) is crucial for the performance under low illumination intensities, a detailed analysis is carried out and it is found that a one-diode model with the R_P being determined from the dark current–voltage characteristics reproduces the behavior quite accurately. Efficiencies of 19.3% on cell level and above 17% on an 8.1 cm^2 module with eight interconnected cells are achieved under 500 lux cold white light-emitting diode illumination.

1. Introduction

In our rapidly developing industry and society, connected machines and intelligent devices are becoming more and more present and important. These technologies and their infrastructure are summarized under the term internet of things (IoT). The number of IoT devices is growing exponentially with an estimated market of about 12.000 Billion USA Dollar in 2030.[1] Already in 2020, the number of IoT devices was calculated to be about 50 Billion, with many of them being used indoors.[2] As a result, an increasing demand of energy is accompanied by that growth. To provide an environmentally friendly power supply for such devices and because of their typically rather low energy consumption local energy-harvesting solutions are suitable options. Alongside thermoelectric and vibrational harvesters, photovoltaics (PV) is a promising way to power indoor IoT devices since dim light sources are often available in the industrial context. Because indoor illumination differs strongly from "1 sun" (air mass 1.5 global, AM1.5G) illumination regarding spectral distribution and intensity, the requirements for the absorber material differ strongly for the two types of illumination. The optimal bandgap of a semiconductor for a maximum efficiency based on the Shockley–Queisser model depends on the input illumination and reflects (among other factors) the tradeoff between non-absorption and thermalization losses.[3] For AM1.5G, the optimal bandgap is about 1.1 eV, which is why crystalline silicon is very well suited for these conditions. In contrast, for example, a typical cold white (cw) light-emitting diode (LED) spectrum at 500 lux (roughly corresponding to 1.4 $W m^{-2}$) shifts to a significantly larger value of about 1.8 eV. This is far beyond the bandgap of crystalline silicon. Therefore, other technologies such as III–V compound systems, amorphous silicon, perovskites, and organic semiconductor materials are considered. However, III–V systems are quite expensive and therefore mainly used in space applications. Organic semiconducting absorber materials cannot only be tailored to match the optimum bandgap for this particular application, but also they are moreover nontoxic and can be processed from nonhalogenated solvents. Due to the small amount of material in combination with an extremely low energy demand for production, organic solar cells are the PV technology with the lowest carbon footprint. All this strongly motivated research on organic solar cells for indoor applications. In addition, the "mild" conditions, that is, low photon dose, no UV radiation, and rather constant,

D. Müller, L. Campos Guzmán, E. Jiang, B. Zimmermann
Fraunhofer Institute for Solar Energy Systems ISE
Heidenhofstr. 2, 79110 Freiburg, Germany

D. Müller, U. Würfel
Freiburg Materials Research Center FMF
University of Freiburg
Stefan-Meier-Str. 21, 79104 Freiburg, Germany
E-mail: uli.wuerfel@ise.fraunhofer.de

E. Jiang, U. Würfel
Cluster of Excellence livMatS
University of Freiburg
Georges-Köhler-Allee 105, 79110 Freiburg, Germany

The ORCID identification number(s) for the author(s) of this article can be found under https://doi.org/10.1002/solr.202200175.

DOI: 10.1002/solr.202200175

moderate temperatures do render potential stability problems of organic PV (OPV) less critical.

In addition to the choice of a suitable absorber, for an ecological and cost-efficient organic solar module, an alternative to the state-of-the-art indium tin oxide (ITO) transparent electrode is beneficial. Fortunately, in the case of indoor illumination, the much lower intensity and thus lower generated current compared to "1 sun" relaxes the electrical conductivity requirements for the transparent electrode, which in turn facilitates the usage of indium-free alternatives.[4,5] In this study, we will present a versatile cell stack, which avoids the use of ITO and proves to deliver promising performances with a large variety of different absorber materials both on the cell and module level.

In literature, numerous reports on the evaluation of new organic absorber materials can be found. Lee et al.[6] reported 28.1% efficiency under 1000 lux with a fluorescent lamp with a fullerene based blend with BTR (long form of all photoactive materials listed in Table S1, Supporting Information) as donor material. However, this value was rebutted by Cui et al. to 19.7% at 1607 lux.[7] Cui et al. presented the wide-gap non-fullerene acceptor material IO-4Cl blended with the donor PM6 with an absorption onset at 1.8 eV resulting in an open-circuit voltage (V_{OC}) above 1 V and a decent efficiency of 24.6% at 500 lux with a warm white (ww)-LED.[7] Recently, Ma et al. published about 29.5% efficiency at 700 lux with a ww-LED incorporating PM6:Y6-O as the absorber material, resulting in a high short-circuit current density (J_{SC}) due to an outstanding external quantum efficiency (EQE), thus compensating for the rather low V_{OC} due to the inappropriate bandgap.[8] However, in all these examples, chloroform (CF) was used as a solvent for the blend layer and the cell architecture incorporated an ITO electrode. Miranda et al.[9] and Liao et al.[10] presented results on organic solar modules with the blend layer blade coated from *o*-xylene-based solutions on ITO-based cell stacks. The first used a fullerene-based ink and achieved up to 15% efficiency on a flexible 7.2 cm^2 active area module at 1000 lux with a ww-LED. The latter used a non-fullerene blend and could reach 21.8% on a rigid 20.4 cm^2 module at 1000 lux with a cw-fluorescent lamp. Huang et al. reported about 20% efficiency on cell level at 1000 lux with a ww-LED for an ITO-free cell stack comprising a polydimethylsiloxane (PDMS)/PEDOT:PSS electrode on a flexible substrate using a polymer:non-fullerene acceptor system (PM6:BTP-4Cl) spin-coated from chlorobenzene.[11]

Lee et al. presented a 100 cm^2 rigid module with an ITO electrode and the fullerene-based Poly[N-9′-heptadecanyl-2,7-carbazole-alt-5,5-(4′,7′-di-2-thienyl-2′,1′,3′-benzothiadiazole)] (PCDTBT):$PCBM_{71}$ absorber coated from chlorobenzene and achieved an efficiency of 11.2% under a 300 lux ww-fluorescent lamp.[12] Arai et al. achieved an efficiency of 17% under a 200 lux ww-LED on a flexible polyethylene terephthalate (PET) substrate with 1DTP-ID:PNP coated from chloroform as absorber material.[13] Zhang et al. show a rigid 10 cm^2 module with CD1:PBN-21 coated from tetrahydrofuran as absorber on an ITO electrode that yields 12% under 1000 lux with a cw-LED.[14]

However, up to now, there are no studies published where the different subtopics, that is, analysis of materials suitable for indoor light harvesting, coating from nonhalogenated solvents in an ITO-free architecture, are tackled simultaneously to fabricate OPV modules. In this work, we present an ITO-free cell stack further developed from what was published earlier by our group.[15,16] It will be shown that it is applicable to a large variety of state-of-the-art organic semiconductors used in OPV. Furthermore, with this cell stack, there is no need for a final vacuum deposition step as the top electrode consists of a highly conductive PEDOT:PSS as hole-transport layer (HTL), followed by a screen printable silver grid, thus being compatible to roll-to-roll processing. In the special case of low indoor light intensities, the printed grid can be avoided completely, which further reduces the costs.

2. Results and Discussion

2.1. Transfer from ITO to ITO-free Architecture

The classical architecture for OPV is a pin superstrate configuration: ITO/HTL/active layer/ETL/metal, usually called standard architecture, with ETL denoting the electron-transport layer. In addition, the often-called inverted architecture ITO/ETL/active layer/HTL/metal with an inverted layer deposition sequence is a nip superstrate configuration and was developed to achieve better stability with a high work function material used as a top contact. In this work, we show that both the standard and the inverted cell stack can be transferred to our ITO-free architecture with a bottom electrode based on aluminum sandwiched between two layers of aluminum-doped zinc oxide (AZO) and a combination of PEDOT:PSS and Ag grid as top contact. **Figure 1** shows a schematic of the three cell stacks. As mentioned earlier in the case of low light illumination, there is no need for a silver grid as the conductivity of the HTL is large enough. All our ITO-free devices for indoor illumination do therefore not comprise a silver grid.

The performance of an organic solar cell does not only rely on the appropriate choice of energy levels at materials/interlayers but also on the deposition sequence. For many of the newly developed active materials, the standard architecture is still the most dominant cell stack. To transfer it to our ITO-free architecture, we have to invert the layer deposition sequence which is often accompanied by adjustments of multiple processing parameters. This includes special treatments of substrate and active material to ensure a proper wetting and a good morphology.[15,17] When it comes to transfer an inverted ITO-based architecture to our ITO-free architecture, there is no need to flip the layer sequence. The former does in most cases comprise a combination of MoO_x and (evaporated) Ag as HTL and hole contact, respectively. This has now to be replaced by PEDOT:PSS as HTL. For some (novel) absorber materials, however, the work function of PEDOT:PSS is too high with respect to the donor's highest occupied molecular orbital (HOMO).[18] This leads to reduced selectivity and hence increased surface recombination at that interface, ultimately resulting in a loss in V_{OC} and fill factor (FF).[19] To overcome that loss, a modified PEDOT:PSS formulation (PV-HTL-5 from Raynergy Tek) with reduced work function (toward more negative values) is used, thus minimizing the losses due to surface recombination, resulting in a higher V_{OC} and FF.[18] **Figure 2** shows the results which are in good agreement with Ref.[18] and thus highlights the necessity of solution processable HTLs with adjusted work function. It should be

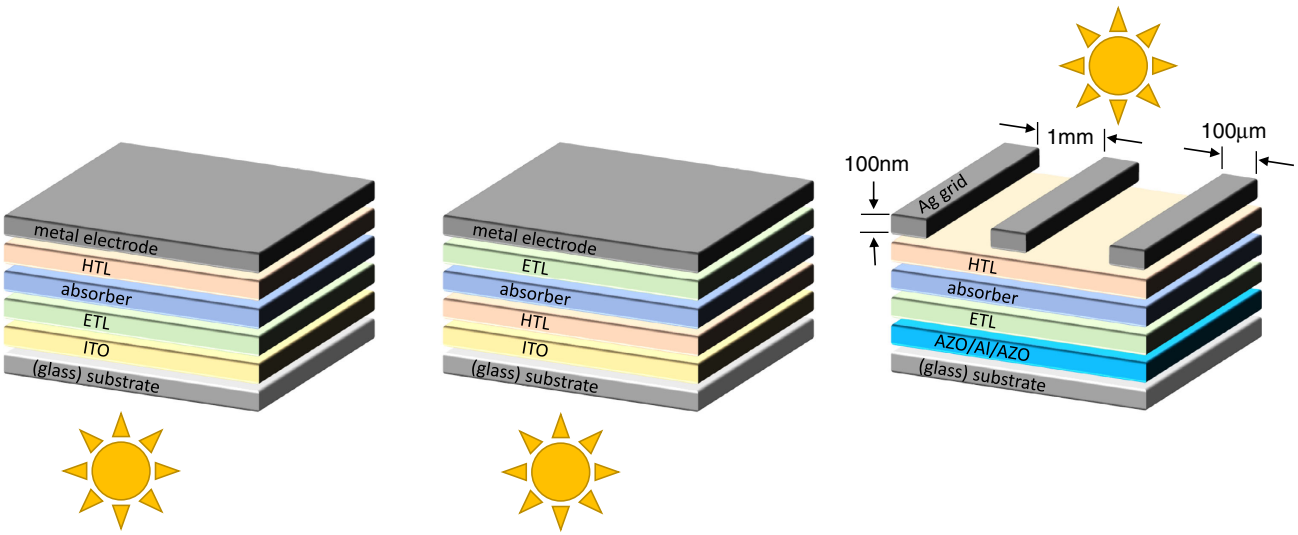

Figure 1. Schematic of the different solar cell architectures, (left) indium tin oxide (ITO) standard, (center) ITO inverted, and (right) ITO free, with the indication of the incoming light.

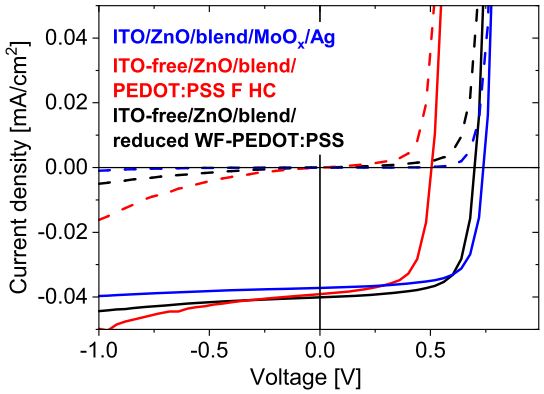

Figure 2. Current density–voltage characteristics for inverted ITO-based (blue) and ITO-free devices with (black) reduced work function and (red) conductive PEDOT:PSS (FHC formulation from Heraeus) with an active area of 0.1 cm^2, comprising TPD-3F:IT-4F as absorber material.

noted that the variation of J_{SC} can be explained with slightly different absorber layer thicknesses as well as different reflections of the two different opaque electrodes, that is, Ag and Al.

We tested a wide range of commercially available active materials. The used solvents include halogenated as well as nonhalogenated ones. **Table 1** compares the performance of ITO and ITO-free solar cells for eight different active materials, measured under 500 lux cw LED (≈6500 K, spectrum given in Figure S1, Supporting Information). We decided only to compare ITO and ITO-free performance values obtained in our own laboratories for the following reasons. Indoor PV is a quite new field and standard test conditions as established since long for outdoor PV (e.g., AM1.5G) are not yet given. The research community has agreed on the proper determination of the intensity and helpful supporting information to be able to qualify measurements of different groups.[20] However, many different lamp types are used and, without properly defined mismatching of the spectra, direct comparisons of absolute values of different groups are rather meaningless. Lübke et al.[21] have made a proposition on how to compare the different values from different groups,

Table 1. Solar cell performance measured under 500 lux 6500 K cold white light-emitting diode (LED), active area 0.1 cm^2 for various absorber materials on indium tin oxide (ITO) and ITO-free architecture.

Active layer	Stack	J_{SC} [µA cm^{-2}]	V_{OC} [V]	FF [%]	PCE [%]	R_P [MΩ cm^2]	Solvent
TPD-3F:IT-4F[10]	ITO	39.2	0.771	70.3	16.0	5.60	O-xylene
	ITO free	47.7	0.679	72.6	16.5	0.73	
PM6:IO–4Cl[7]	ITO	34.8	1.02	65.1	16.3	1.80	Chloro benzene
	ITO free	38.3	0.987	63.3	16.8	71.00	
PM6:Y6	ITO	57.8	0.639	64.0	16.6	0.18	Chloroform
	ITO free	47.5	0.569	52.0	9.90	3.50	
BTR:PCBM[6]	ITO	42.7	0.718	73.3	15.0	16.20	Chloroform
	ITO-free	51.1	0.712	62.9	16.1	30.00	O-xylene
PM6:DTY6[23]	ITO free	42.5	0.592	69.3	12.3	13.20	O-xylene
ATL3	ITO	54.4	0.541	33.9	7.02	0.95	O-xylene based
	ITO free	38.4	0.604	62.5	10.2	4.81	
PV-X plus[27]	ITO	54.5	0.671	63.1	16.3	0.39	O-xylene
	ITO free	53.3	0.672	76.6	19.3	113.04	
D18:Y6	ITO	53.6	0.604	69.0	15.7	1.48	Chloroform
	ITO free	50.3	0.584	65.1	13.4	7.33	

given the spectra, EQE and J_{SC} values are presented. The biggest challenge here will be to measure an absolute EQE.[22]

For the absorber materials TPD-3F:IT-4F and PM6:IO-4Cl, there is almost no difference in performance between the ITO and ITO-free layer stack. The ITO-based reference architecture from literature for the first absorber material is inverted and for the latter it is the standard one.[7,10]

For the BTR:$PCBM_{71}$ system, we see comparable results on ITO and on ITO-free architectures, with a minor improvement on the ITO-free stack. This improvement is especially remarkable since we were able to obtain it even after the transition from a chlorinated to a non-chlorinated solvent for the active layer.

For PM6:Y6 spin-coated from chloroform (CF), we found a large difference in efficiency between the ITO and ITO-free architecture. It has to be mentioned that our main focus of this work is on active materials specially designed for indoor light harvesting (i.e., with an EQE onset of about 700 nm) and the PM6:Y6 blend processing was not optimized in the same way as for other materials. Interesting is however that even though PM6:Y6 is a very good candidate for converting sunlight with an EQE onset of about 900 nm, it shows similar performance (on ITO) as other active materials specially designed for artificial light harvesting (e.g., BTR,[6] PM6:IO-4Cl[7]).

For PM6:DTY6, the counterpart to PM6:Y6 which gives good performance coated from o–xylene, a decent performance of 12.3% was achieved under 500 lux.[23] However, in the case of the ITO-free devices, we were not able to fabricate a sample which was not severely limited by the parallel resistance (R_P), thus a proper comparison was not possible and the data is not shown in the table.

The up-to-now record efficiency binary material in OPV under "1 sun" is D18:Y6.[24–26] It also yields decent performances at 500 lux cw LED light, both on ITO and our ITO-free cell stack.

PV-X plus, a ternary donor:acceptor:acceptor blend showed the highest efficiencies at 500 lux on the ITO-free architecture of 19.3%.[27] This value is to the best of our knowledge, the highest value reported for ITO-free indoor organic solar cells. PV-X plus benefits from a broad and high EQE, however, lacks the blue region. As a result, the current for cw LED illumination might be significantly reduced compared to redshifted warm white LEDs. With an EQE onset of ≈900 nm, also the maximum V_{OC} is limited.

These results demonstrate that both ITO-based cell stacks can be successfully transferred to our ITO-free architecture for a large variety of absorber materials.

In Table 1, the parallel resistance extracted from the inverse slope of the dark current density–voltage (JV) curve at 0 V was added. In Section 2.2, we will elaborate the parallel resistance influence in depth and show that for parallel resistance values $>10^5\,\Omega\,cm^2$ its influence on the efficiency becomes negligible. This is the case for all samples presented in Table 1, which allows for a fair comparison between architectures and absorber material.

2.2. Device Upscaling on Rigid and Flexible Substrates

As a next step, the solar cells were upscaled from 0.1 to 1.1 cm^2 active area and further to 8.1 cm^2 modules (8 cells interconnected in series). These larger solar cells and also modules were fabricated by both spin-coating and slot-die coating, as well as on different substrate types: glass and flexible barrier films, the latter from 3M (UBF 512), from Krempel (HBF 772), from Amcor (SOLARS-AUGW), and also on a non-barrier flexible film from Melinex (ST 504). The upscaling from 0.1 to 8.1 cm^2 as well as the coating on different substrate materials could be realized without prominent losses in performance as can be seen in **Figure 3**. Furthermore, the transition from spin-coating to slot-die coating was done successfully. **Figure 4** shows the intensity-dependent efficiency and the corresponding current–voltage characteristics for an ITO-free PV-X plus–based module measured under cw LED light. Since the module layout is designed for low intensities, we only used a conductive PEDOT:PSS formulation as a top contact, that is, no silver grid was applied. For this reason, the series resistance is expected to limit the performance toward higher intensities, which was however not visible in our measurements up to 1000 lux where a high PCE of 17% was achieved. In contrast, toward lower intensities, the performance becomes limited due to the impact of a finite parallel resistance. Nevertheless, the presented module still shows an efficiency of above 13% at a very low intensity of 50 lux.

2.3. Impact of Parallel Resistance on Low-Intensity Performance

The importance of a high parallel resistance (R_P) for a good solar cell performance under low intensity illumination was already discussed elsewhere.[5,28–31] Different groups stated different absolute values, for example, Steim et al. published 85 $k\Omega cm^2$ as a minimum requirement for the R_P not to be limiting under a cw-fluorescent lamp (light color 830) at 1000 lux.[5] Proctor et al. argued for R_P values greater than 1 $M\,\Omega\,cm^2$ for light intensities less than 1 sun.[28] Lechêne et al. tried a different approach to qualify the potential of organic solar cells for the use under indoor light conditions. Namely, they calculated the ratio $J_{dark}/J_{SC,AM1.5G}$, which should be equal to $P_{lowlight}/P_{AM1.5G}$, with J_{dark} denoting the dark current density and P the incident radiative power.[32] This would lead to a limiting R_P value depending on the J_{SC}, which is usually different for different absorber materials. Thus, they stated that the R_P is less meaningful to determine if the lowlight performance of a solar cell is limited by it or not. We however found an excellent agreement between our experimental data and calculations based on the one-diode model, see **Figure 5**a. The simulated curves (solid lines) are based on the Shockley–Queisser model with a bandgap of 1.78 eV, which is optimal for the 500 lux indoor spectrum, with an added parallel resistance (cf. Equation (1)). As can be seen, for "1 sun" illumination, $R_P > 2000\,\Omega\,cm^2$ is sufficient to ensure no noticeable losses and for $R_P = 100\,\Omega\,cm^2$ about 50% performance loss is observed. In strong contrast, for 500 lux LED illumination a very high R_P of at least $10^6\,\Omega\,cm^2$ is required to render losses negligible and for $R_P = 2 \times 10^4\,\Omega\,cm^2$ the performance is reduced by about 50%. The experimental data has of course much lower absolute values, but the impact of the parallel resistance is in excellent agreement with the simulated data. For the experimental data, we extracted the R_P from the inverse slope of the dark current–voltage characteristics around 0 V. Note that since the dark currents are (ideally) very small, already minor (absolute) fluctuations cause large differences in the calculated R_P values. The number of datapoints in this voltage range as well

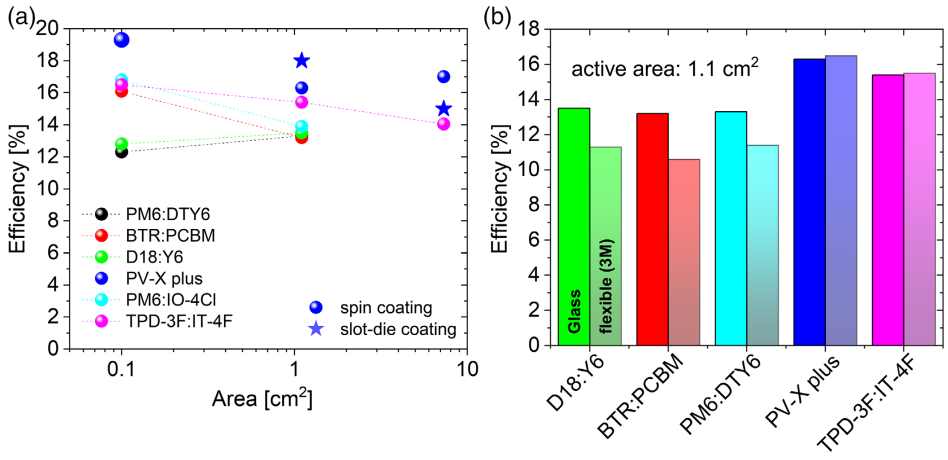

Figure 3. a) Solar cell and module performance with respect to the active area measured at 500 lux with a cold white light-emitting diode (LED) for different absorber materials. b) Comparison of rigid and flexible solar cells for various absorber materials.

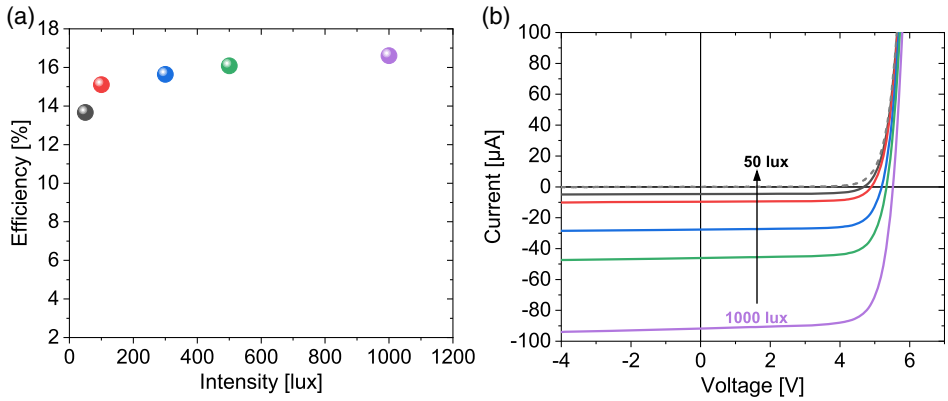

Figure 4. Performance a) and current density–voltage (*JV*) curves b) of an ITO-free photovoltaics (PV)-X plus–based 8.1 cm^2 spin-coated module measured at several cold white LED intensities.

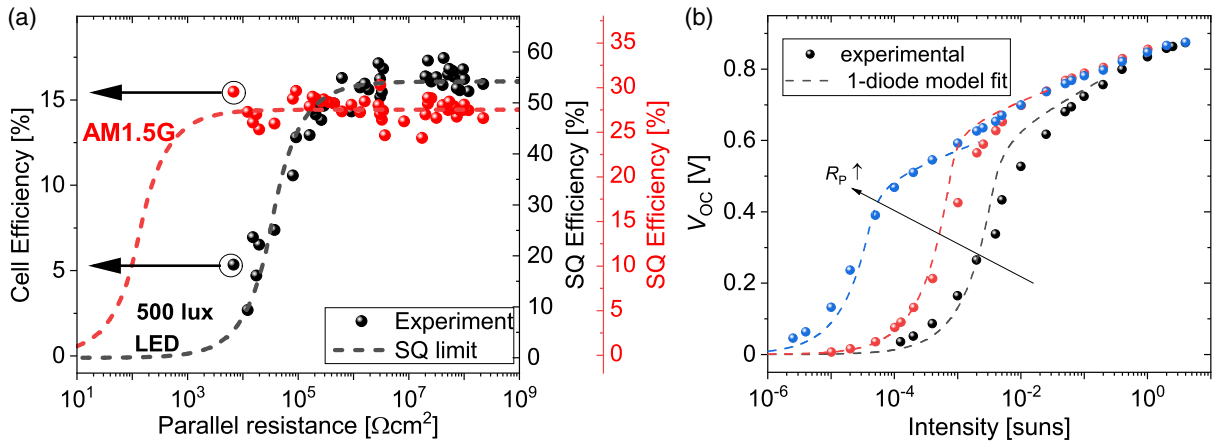

Figure 5. a) Solar cell efficiency (ITO-free, PV-X plus, 0.1 cm^2 active area) as a function of the parallel resistance for two different illumination sources. b) Open-circuit voltage (V_{OC}) as a function of light intensity (green LED) for three solar cells with different shunt resistance (pin ITO stack, D18:Y6, 0.1 cm^2 active area).

as the integration time for each measured datapoint will therefore influence the calculated values. Nevertheless, in most cases, it is a good measure to determine if the performance is strongly limited due to the parallel resistance or rather due to other factors.

A large R_P over the whole device area is especially important for larger cells and modules. On larger areas, the probability of local shunts is increased. On module level, a (partially) shunted cell will reduce the device's FF and voltage without showing a prominent slope in the dark current. For module fabrication, the shunt control has to be done by luminescence[30] or thermography.[33] Figure 5a shows the data of a batch of nine substrates with similar 0.1 cm^2 solar cells, it represents thereby a random spatial probing of the area, since each substrate has a size of 2.5×2.5 cm^2 and contains six individual solar cells. Although the majority of these cells shows a decent R_P on a module level, it could lead to significant losses. For the origin of low R_P values, several explanations exist. A quite recent study on perovskite solar cells tries to distinguish between pinholes only in the absorber layer (ETL:HTL contact, causing an "exponential" shunt, flat JV curve around 0 V, but reduced FF) and pinholes through ETL, HTL, and absorber layer resulting in a contact of the highly conductive top and bottom electrodes and thus in a typically ohmic shunt.[34] Crucial for a shunt-free device is a closed absorber layer, which requires a smooth ETL or HTL underneath. The closed absorber film also depends on other factors such as the wettability of the layer below surface tensions, which can be modified by surfaces treatments (e.g., solvent washing) or side-chain modifications of the active material and of course, any unwanted (dust) particle on the surface.

In Figure 5b, intensity-dependent V_{OC} measurements of different 0.1 cm^2 D18:Y6-based solar cells on an ITO electrode are shown and plotted together with the one-diode equation with the parallel resistance obtained from the dark current as explained earlier. We used the one-diode equation (Equation 1) with neglected series resistance. J_0, n_{id}, k_B, T, q, V, and J denote the dark saturation current density, ideality factor, Boltzmann constant, temperature, electron charge, voltage, and current density, respectively. Under V_{OC} conditions ($J = 0$), Equation (1) can be resolved analytically for V_{OC} as done in Equation 2, with W denoting the Productlog function. The ideality factor n_{id} is extracted from the slope of the intensity-dependent V_{OC} data around 1 sun where it is not yet influenced by the R_P. J_0 is obtained the dark JV curves. The V_{OC} decreases depending on the present recombination mechanism (n_{id}) with decreasing light intensity. At some point, this logarithmic trend turns over into an R_P-dominated voltage reduction. As expected, the transition region where the R_P dominates shifts toward lower light intensities for larger R_P values. The calculated V_{OC} values from Equation (2) reproduce the experimental data very well. From this, we conclude that the simple one-diode model is sufficiently accurate to determine the value of the parallel resistance independent of what its real physical origin is.

$$J(V) = J_0\left(\exp\left(q\frac{V}{n_{id}k_BT}\right) - 1\right) - J_{SC} + \frac{V}{R_P} \quad (1)$$

$$V_{OC} = \frac{-n_{id}k_BTW\left(\frac{\exp\left(\frac{(J_0+J_{SC})qR_P}{n_{id}k_BT}\right)J_0qR_P}{n_{id}k_BT}\right) + J_0qR_P + J_{SC}qR_P}{q} \quad (2)$$

3. Conclusion

In this work, we present an ITO-free solar cell stack, which is proven to be very suitable for indoor OPV. A large variety of novel absorber materials were tested on that cell stack efficiencies measured under 500 lux with a cw LED were found to be comparable to those achieved on the conventional ITO architecture. The influence of the parallel resistance on the low-intensity illumination performance was evaluated in detail. It confirms the requirement of a defect (shunt)-free absorber layer for larger area devices and modules under indoor illumination. We also showed that the R_P extracted from the dark JV curves matches well with what is obtained by intensity-based open-circuit voltage measurements. The highest indoor efficiency on cell level of 19.3% was realized with PV-X plus as the absorber material using *o*-xylene as solvent. Further, we successfully scaled up from small 0.1 cm^2 lab cells by spin-coating toward 8.1 cm^2 modules with eight serially connected cells manufactured by slot-die coating, while maintaining the conversion efficiency at a high level of 17% at 500 lux. The modules deliver a total power of about 200 µW with a voltage of about 5 V, which is suitable for many low-power IoT applications and even at 50 lux the efficiency is still larger than 13%.

4. Experimental Section

Device Fabrication and Characterization: The fabrication of ITO-based devices started on structured 25×25 mm^2 ITO-coated glass substrates from Kintec with a sheet resistance of 15 Ω. Cleaning in ultrasonic baths of acetone, isopropanol, and water for 10 min each and subsequent nitrogen dry blowing and UV-ozone treatment for 20 min were performed. A 40 nm film of PEDOT:PSS (AI 4083 from Heraeus) was spin-cast in air and annealed for 15 min at 150 °C in a nitrogen-filled glove box (GB). For the inverted cell stack, a 15 nm ZnO (1% N11 from Avantama, diluted in isopropanol) was spin-cast in air and annealed in a GB for 5 min at 120 °C. A 130 nm film of PV-X plus (from Raynergy Tek) spin-cast from *o*-xylene at room temperature (RT) followed by 5 min annealing at 120 °C formed the active layer, see Table S2 and S3, Supporting Information, for further details also on the other active materials. A 20 nm Ca layer followed by 100 nm Al or 8 nm MoO_x layer followed by 100 nm Ag, for the standard and inverted architecture, respectively, was deposited via thermal evaporation at a pressure below 10^{-5} mbar with a shadow mask.

The ITO-free cells and module fabrication process started with glass substrates, after the same cleaning procedure as mentioned earlier, an Al-based metal electrode was deposited via sputtering with a shadow mask. Optional ETL as well as the active layer steps are similar as mentioned previously, see also Table S2, Supporting Information. The HTL was formed by a double layer of work function (WF)-modified PEDOT:PSS (30 nm PV-HTL-X and 50 nm PV-HTL-5, from Raynergy Tek; the sheet resistance is 795 ± 137 Ω and the transmission is plotted in Figure S2, Supporting Information) spin-cast in a GB and dried for 5 min at 110 °C in the GB. For the cells for electrical connection, a support structure consisting of 5 nm Cr and 100 nm Ag was deposited via e-beam and thermal evaporation, respectively, at a pressure below 10^{-5} mbar with a shadow mask.

The modules were structured as follows: P2 (HTL, absorber and ETL removal to contact bottom and top electrode of two adjacent cells) and P3 (HTL, and optional absorber and ETL, removal to interrupt the top contact) were realized with a thread soaked in solvent in a custom setup. Finally, a 100 nm Ag cell interconnection was deposited via thermal evaporation by a shadow mask. Details on the module layout can be found in Figure S3, Supporting Information.

Current voltage measurements at simulated AM1.5G light by a class A solar simulator (Newport SP94063A-SR1-167) and different indoor intensities by a 6000 K LED spotlight (LTAS-100/1 from Brandmaier) with protection against ambient light were carried out with a computer-programmed Keithley 2400 source meter^{-1}. The indoor intensity was determined according to Cui et al. The lamp spectrum and luminosity function are given in Figure S1, Supporting Information.[20] To measure the intensity, we used a certified reference solar cell (RS-ID-4).

Supporting Information

Supporting Information is available from the Wiley Online Library or from the author.

Acknowledgements

The authors acknowledge the funding from the German Federal Ministry for Economic Affairs and Energy (FKz. 03EE1007—Organaut). Cluster of Excellence livMatS: Funded by the Deutsche Forschungsgemeinschaft (DFG, German Research Foundation) under Germany's Excellence Strategy—EXC-2193/1—390951807.

Open Access funding enabled and organized by Projekt DEAL.

Data Availability Statement

The data that support the findings of this study are available from the corresponding author upon reasonable request.

Conflict of Interest

The authors declare no conflict of interest.

Keywords

flexible, green solvents, indoor, IoT, ITO-free, OPV modules, parallel resistance

Received: February 23, 2022
Revised: March 17, 2022
Published online: April 10, 2022

[1] S. Al-Sarawi, M. Anbar, R. Abdullah, A. B. Al Hawari, in *2020 Fourth World Conf. on Smart Trends in Systems, Security and Sustainability (WorldS4)*, IEEE, London, UK **2020**, p. 449.
[2] C. Perera, C. H. Liu, S. Jayawardena, M. Chen, *IEEE Access* **2014**, *2*, 1660.
[3] W. Shockley, H. J. Queisser, *J. Appl. Phys.* **1961**, *32*, 510.
[4] D. Glowienka, Y. Galagan, *Adv. Mater.* **2022**, *34*, e2105920.
[5] R. Steim, T. Ameri, P. Schilinsky, C. Waldauf, G. Dennler, M. Scharber, C. J. Brabec, *Sol. Energy Mater. Sol. Cells* **2011**, *95*, 3256.
[6] H. K. H. Lee, J. Wu, J. Barbé, S. M. Jain, S. Wood, E. M. Speller, Z. Li, F. A. Castro, J. R. Durrant, W. C. Tsoi, *J. Mater. Chem. A* **2018**, *6*, 5618.
[7] Y. Cui, Y. Wang, J. Bergqvist, H. Yao, Y. Xu, B. Gao, C. Yang, S. Zhang, O. Inganäs, F. Gao, J. Hou, *Nat. Energy* **2019**, *4*, 768.
[8] L.-K. Ma, Y. Chen, P. C. Y. Chow, G. Zhang, J. Huang, C. Ma, J. Zhang, H. Yin, A. M. Hong Cheung, K. S. Wong, S. K. So, H. Yan, *Joule* **2020**, *4*, 1486.
[9] B. H. S. Miranda, L. D. Q. Corrêa, G. A. Soares, J. L. Martins, P. L. Lopes, M. L. Vilela, J. F. Rodrigues, T. G. Cunha, R. D. Q. Vilaça, S. Castro-Hermosa, L. Wouk, D. Bagnis, *Sol. Energy* **2021**, *220*, 343.
[10] C.-Y. Liao, Y. Chen, C.-C. Lee, G. Wang, N.-W. Teng, C.-H. Lee, W.-L. Li, Y.-K. Chen, C.-H. Li, H.-L. Ho, P. H.-S. Tan, B. Wang, Y.-C. Huang, R. M. Young, M. R. Wasielewski, T. J. Marks, Y.-M. Chang, A. Facchetti, *Joule* **2020**, *4*, 189.
[11] J. Huang, Z. Ren, Y. Zhang, K. Liu, H. Zhang, H. Tang, C. Yan, Z. Zheng, G. Li, *Adv. Funct. Mater.* **2021**, *31*, 2010172.
[12] H. K. H. Lee, Z. Li, J. R. Durrant, W. C. Tsoi, *Appl. Phys. Lett.* **2016**, *108*, 253301.
[13] R. Arai, S. Furukawa, N. Sato, T. Yasuda, *J. Mater. Chem. A* **2019**, *7*, 20187.
[14] Y. Zhang, N. Wang, Y. Wang, J. Zhang, J. Liu, L. Wang, *iScience* **2021**, *24*, 103104.
[15] M. Glatthaar, M. Niggemann, B. Zimmermann, P. Lewer, M. Riede, A. Hinsch, J. Luther, *Thin Solid Films* **2005**, *491*, 298.
[16] D. Kaduwal, H.-F. Schleiermacher, J. Schulz-Gericke, T. Kroyer, B. Zimmermann, U. Würfel, *Sol. Energy Mater. Sol. Cells* **2014**, *124*, 92.
[17] B. Zimmermann, *Inversion of the Layer Sequence in Organic Solar Cells - Physical and Technological Aspects*, PhD thesis, University of Freiburg, **2008**.
[18] N.-W. Teng, C.-H. Li, W.-C. Lo, Y.-S. Tsai, C.-Y. Liao, Y.-W. You, H.-L. Ho, W.-L. Li, C.-C. Lee, W.-C. Lin, Y.-M. Chang, *Sol. RRL* **2020**, *4*, 2000223.
[19] J. Reinhardt, M. Grein, C. Bühler, M. Schubert, U. Würfel, *Adv. Energy Mater.* **2014**, *4*, 1400081.
[20] Y. Cui, L. Hong, T. Zhang, H. Meng, H. Yan, F. Gao, J. Hou, *Joule* **2021**, *5*, 1011.
[21] D. Lübke, P. Hartnagel, J. Angona, T. Kirchartz, *Adv. Energy Mater.* **2021**, *11*, 2101474.
[22] E. A. Katz, A. Mescheloff, I. Visoly-Fisher, Y. Galagan, *Sol. Energy Mater. Sol. Cells* **2016**, *144*, 273.
[23] S. Dong, T. Jia, K. Zhang, J. Jing, F. Huang, *Joule* **2020**, *4*, 2004.
[24] U. Würfel, J. Herterich, M. List, J. Faisst, M. F. M. Bhuyian, H.-F. Schleiermacher, K. T. Knupfer, B. Zimmermann, *Sol. RRL* **2021**, *5*, 2000802.
[25] M. A. Green, E. D. Dunlop, J. Hohl-Ebinger, M. Yoshita, N. Kopidakis, X. Hao, *Prog. Photovoltaics Res.* **2021**, *29*, 657.
[26] Q. Liu, Y. Jiang, K. Jin, J. Qin, J. Xu, W. Li, J. Xiong, J. Liu, Z. Xiao, K. Sun, S. Yang, X. Zhang, L. Ding, *Sci. Bull.* **2020**, *65*, 272.
[27] C.-Y. Liao, Y.-T. Hsiao, K.-W. Tsai, N.-W. Teng, W.-L. Li, J.-L. Wu, J.-C. Kao, C.-C. Lee, C.-M. Yang, H.-S. Tan, K.-H. Chung, Y.-M. Chang, *Sol. RRL* **2021**, *5*, 2000749.
[28] C. M. Proctor, T.-Q. Nguyen, *Appl. Phys. Lett.* **2015**, *106*, 83301.
[29] M. A. Saeed, S. H. Kim, H. Kim, J. Liang, H. Y. Woo, T. G. Kim, H. Yan, J. W. Shim, *Adv. Energy Mater.* **2021**, *11*, 2003103.
[30] M.-A. Llobel, G. Rivière, C. Arrivé, S. Courtel, G. Vannier, S. Cros, M. Matheron, *Sol. RRL* **2021**, *5*, 2000634.
[31] J. Bachmann, C. Buerhop-Lutz, R. Steim, P. Schilinsky, J. A. Hauch, E. Zeira, C. J. Brabec, *Sol. Energy Mater. Sol. Cells* **2012**, *101*, 176.
[32] B. P. Lechêne, M. Cowell, A. Pierre, J. W. Evans, P. K. Wright, A. C. Arias, *Nano Energy* **2016**, *26*, 631.
[33] F. Frühauf, O. Breitenstein, *Sol. Energy Mater. Sol. Cells* **2017**, *169*, 195.
[34] P. Kaienburg, P. Hartnagel, B. E. Pieters, J. Yu, D. Grabowski, Z. Liu, J. Haddad, U. Rau, T. Kirchartz, *J. Phys. Chem. C* **2018**, *122*, 27263.